ARTICLES

Observation of the shadows of the Moon and Sun using 100 TeV cosmic rays

A. Borione,[1] M. Catanese,[2] C. E. Covault,[1] J. W. Cronin,[1] B. E. Fick,[1] K. G. Gibbs,[1]
K. D. Green,[2] S. Hauptfeld,[1] D. Kieda,[3] H. A. Krimm,[1,*] N. C. Mascarenhas,[1,†] J. Matthews,[2] T. A. McKay,[1,‡]
D. Müller,[1] B. J. Newport,[1] D. Nitz,[2] R. A. Ong,[1] L. J Rosenberg,[1,§] D. Sinclair,[2] and J. C. van der Velde[2]
[1]*Enrico Fermi Institute, University of Chicago, Chicago, Illinois 60637*
[2]*Department of Physics, University of Michigan, Ann Arbor, Michigan 48109*
[3]*Department of Physics, University of Utah, Salt Lake City, Utah 84112*
(Received 12 March 1993)

The Chicago Air Shower Array has imaged the shadows of the Moon and Sun and measured the angular diameter of the Moon with cosmic rays having energies above about 100 TeV. The shadow of the Sun shows effects attributed to the curvature of cosmic rays by the solar magnetic field. This study verifies that our direction reconstruction has no serious systematic errors, and provides a measure of the angular resolution of the array.

PACS number(s): 96.40.De, 96.40.Pq, 96.50.Bh

I. INTRODUCTION

The Chicago Air Shower Array (CASA) is a large ground-based scintillation detector [1–4]. It is located at the Dugway Proving Ground is west central Utah, latitude 40°N and mean atmospheric depth 870 g/cm^2. A schematic aerial view of CASA is shown in Fig. 1. Each dot represents one scintillation station of the array. The scintillator stations, each containing four sheets of 61 cm$\times$61 cm$\times$1.3 cm acrylic, are spaced 15 m apart and covered by one radiation length of lead. The boundary of the array encloses 2.3×10^5 m^2. Shown, but not used directly in this study, is a buried muon array consisting of 2560 m^2 of underground scintillation detectors (solid boxes), and an array of four Čerenkov telescopes (circles). Construction of CASA began in 1989 with the installation of a prototype 49 station array, and results from this prototype have been previously reported [5]. An array of 529 stations (with the boundary represented by the dashed line) was operational by early 1990 and continued to take data through commissioning of the complete 1089 station array in early 1991. The nominal trigger rate of the complete array is 25 Hz and, on average, 19 stations record data from each triggered event.

An important goal of CASA is the search for point sources of ultrahigh-energy (energy greater than about 100 TeV) cosmic rays. These cosmic rays produce extensive air showers in the atmosphere and are detected when the axis (the shower "core") of a sufficiently energetic shower lands within the boundary of the array. Close to the core, particles making up the shower arrive at CASA stations in a thin disk. For each shower, the set of time differences between adjacent CASA stations determines

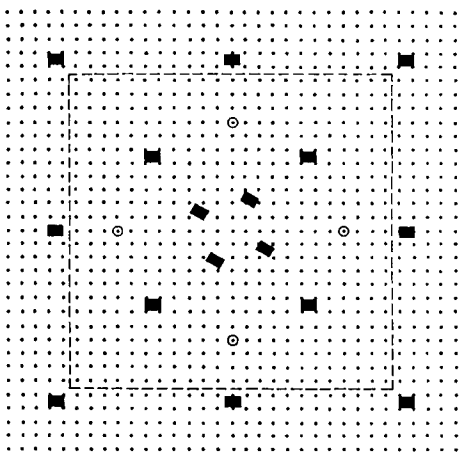

FIG. 1. Schematic aerial view of the CASA experiment, located at latitude 40°N, at a nominal atmospheric depth of 870 g/cm^2. Each dot represents one scintillation station of the array. The scintillator stations are spaced 15 m apart. The boundary of the array encloses 2.3×10^5 m^2. The solid boxes represent a total of 2560 m^2 of underground muon scintillation detectors. The circles represent Čerenkov telescopes. The dashed line encloses the 529 stations used in this analysis.

*Present address: Center for Space Research, Massachusetts Institute of Technology, Cambridge, MA 02139.
†Present address: Norman Bridge Laboratory of Physics, California Institute of Technology, Pasadena, CA 91125.
‡Present address: Fermi National Accelerator Laboratory, Batavia, IL 60510.
§Present address: Department of Physics, Massachusetts Institute of Technology, Cambridge, MA 02139.

the shower arrival direction. A point source is inferred from an excess of showers arriving from a particular direction of the celestial sphere. Because of the finite instrument resolution, showers from a point source appear to arrive from a finite region of the sky and are therefore accompanied by a background of nearly isotropic cosmic rays. An accurate determination of both signal and background from a particular direction therefore requires a good understanding of both detector accuracy and precision.

An important parameter for these searches is the angular resolution of the experiment—the better the angular resolution, the smaller the required search region around a putative source, and thus the lower the background. The angular resolution depends on the number of shower particles striking the ground (the shower "size"), the distance of the shower core from the boundary of the array, and the zenith angle of the shower axis.

We have not, so far, observed a significant excess of air showers from any selected direction in our searches. These negative observations would be strengthened considerably by a demonstration that CASA could indeed detect a fiducial source. Unfortunately, no such definitive source is apparent at energies above the CASA cosmic ray energy threshold near 100 TeV [6]. However, as first suggested by Clark in 1957 [7], the cosmic ray antisource of the Moon or Sun may be treated as a fiducial object. The apparent angular diameter of the Sun and Moon is about $\frac{1}{2}°$, comparable to the characteristic CASA angular resolution at large shower size. The shadowing of cosmic rays from the direction of the Sun or Moon is therefore useful in measuring the CASA angular resolution directly, without the need to invoke Monte Carlo simulations. Observing the expected depth of shadowing also verifies the array pointing accuracy and stability.

CASA is the largest detector of its kind, and the accumulated CASA data set is the largest in the world (and growing by nearly 10^9 events per year). Prior observations of the Moon and Sun shadow have been made using a much smaller data sample [8] or at lower energy [9]. Observing the shadow of the Moon and Sun cast in 100 TeV cosmic rays is an important step in validating our present and future results, and refinement of the technique may eventually give information about primary cosmic ray composition and solar magnetic fields.

Almost all the cosmic rays are charged and therefore bend under the influence of solar and terrestrial magnetic fields. Particles with smaller total energy or larger electric charge have lower magnetic rigidity and will bend more. Let us consider a cosmic ray proton moving backwards along an Earth to Moon trajectory. The transverse momentum imparted to the cosmic ray proton by the Earth's magnetic field (with equitorial dipole field strength 0.5 G at a radius 6.4×10^3 km) is approximately $\Delta P = 5\times10^{10}$ eV/c. As examples, a cosmic ray proton with energy 100 TeV will therefore deflect in angle by $5\times10^{10}/10^{14}=0.03°$, and a cosmic ray iron nucleus will deflect in angle by $26\times5\times10^{10}/10^{14}=0.7°$ along the Earth to Moon trajectory. This angular deflection is negligible for the case of protons with energy near the CASA threshold, but for iron is comparable to the CASA angular resolution. Now consider a cosmic ray proton moving along a trajectory from the center of the Sun (with equitorial dipole field 3 G at a radius 700×10^3 km) to the center of the Earth. The transverse momentum imparted to the proton and angular deflection is 3×10^{13} eV/c and 17° at 100 TeV, and the radius of curvature of a cosmic ray iron nucleus is less than one astronomical unit (AU). Note that this example should be treated with caution as a trajectory from the center of the Sun to the center of the Earth is unphysical (a more realistic trajectory is one just grazing the photosphere). Also, the solar magnetic field is strongly influenced by the solar wind and shows large deviations from a pure dipole, especially in the epoch when data for this analysis were taken [10]. While these effects complicate a quantitative estimate of the effects of the solar magnetic field on cosmic rays, we do have the qualitative picture of small deflections of cosmic rays grazing the Moon, and larger deflections of cosmic rays grazing the Sun.

II. EVENT SELECTION

The data sample used in this study includes all CASA events recorded between March 1990 and April 1991, some 420 million events. For most of this time, CASA consisted of 529 stations, though later more stations were added. The nominal trigger rate grew from 8 Hz in the early part of this period to 12 Hz for most of the time, eventually reaching 25 Hz when the array was complete. The initial rate increase was due to hardware changes in the trigger system and reduced detector maintenance dead time. The later rate increase was due to increased area from additional stations. Note, however, that only data with cores landing within the inner 529 stations are used in this analysis.

The first stage of processing consisted of applying timing and gain calibrations to the raw data, thereby determining the number of charged particles crossing each counter and the shower front timing differences between adjacent CASA stations. In the second stage of processing, about 20% of the showers were discarded; these were mostly small showers where there was not enough information to determine even a crude arrival direction.

For each coordinated universal (UTC) event time, based on redundant earth station (WWVB) and satellite (GOES) clocks, each with an absolute accuracy of better than 1 ms, the geocentric apparent positions of the center of the Moon and Sun are computed (all positions are computed at the epoch of the shower). These predicted positions result from Bessel's second-order interpolation of tabulated daily coordinates [11] and are generally accurate to better than 0.01° in space angle. The geocentric direction of the Moon is transported to the topocentric direction at the CASA site, correcting the parallax introduced by the Earth radius.

This processing resulted in approximately 4.7 million events arriving within a 12° space angle of the center of the Moon or Sun. Some of these events were discarded for one or more of the following reasons: The timing circuitry in individual stations is nonlinear for time delays corresponding to showers arriving from very low alti-

tudes. Rather than correcting this nonlinearity, we eliminate events arriving from altitudes below 30°, affecting some 0.1% of the events. Output from a faulty processor was discarded, eliminating 3.7% of the events. Nearby lightning storms damaged station circuitry in the eastern portion of the array and data from this period of time are eliminated, affecting 5.1% of the events. Finally, 0.2% of the events do not contain enough data to provide a reliable shower size and are removed. We expect the determination of the shower arrival direction to suffer for showers with cores landing near or beyond the array boundary due to multiple scattering, low particle density, and curvature of the shower front. We therefore remove from the remaining 4.3 million events those with cores landing outside the square edge 15 m inside the boundary of the array. This core cut retains 2.8 million events. The event yields from this selection procedure are in agreement with yields expected from convolving the measured altitude distribution of showers, the altitude distribution of the Moon and Sun, and the CASA live time.

III. SHADOWING

The deficit due to cosmic rays striking the Moon and Sun is apparent in Fig. 2, where we show the number of events in annuli of constant solid angle (with first bin $\frac{1}{2}°$ wide) centered on the (a) Moon and (b) Sun. There are no additional shower size cuts applied to these data. The shadowing appears as the deficit near 0°. We then look at a region of the sky where there is nothing to shadow the cosmic rays: For each shower, we generate azimuth directions for these fake Moons and Suns by rotating the actual position of the Moon and Sun around the vertical axis by ±8° in space angle. Since the event yield of CASA is nearly uniform in azimuth, the fake objects provide internal estimates of the number of showers expected from near the direction of the Moon and Sun. The number of events near the fake objects is shown in Figs. 2(c) and 2(d). That no deficit appears for the fake objects demonstrates that the deficits in Figs. 2(a) and 2(b) are not an artifact. We use half the averaged bin contents from the fake-objects in Figs. 2(c) and 2(d) as an estimate of the background levels in Figs. 2(a) and 2(b). This number of background events, the number of events in the first bin of Figs. 2(a) and 2(b), and the significance of this first bin deficit according to the Li and Ma statistic [12] are shown in Table I.

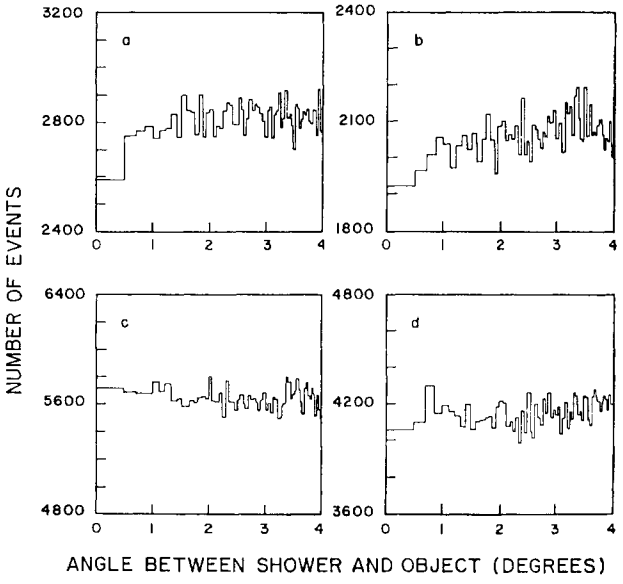

FIG. 2. The number of events in annuli of constant solid angle (the bin at the far left is $\frac{1}{2}°$ wide) centered on the (a) Moon, (b) Sun, (c) two fake Moons, and (d) two fake Suns. Shadowing is evident in (a) and (b) as a deficit at 0°.

TABLE I. The number of signal and background events in the first angular bin from the center of the Moon and Sun.

	Number of events in first bin	Number of background events	Significance of first bin deficit
Moon	2589	2819.4	4.3σ
Sun	1921	2076.2	3.4σ

As suggested earlier, we expect the quality of the determination of the shower arrival direction to improve as the shower size increases. To test this assumption, we apply a shower size cut, retaining those events with $\log_{10}$(shower size) > 4.5. The shower size cut retains 1.6 million events. The deficit due to cosmic rays striking the Moon and Sun is shown in Fig. 3. Note that here the first bin is $\frac{1}{4}°$ wide, whereas the first bin in Fig. 2 is $\frac{1}{2}°$ wide. The resolution obtained for these large showers is visibly

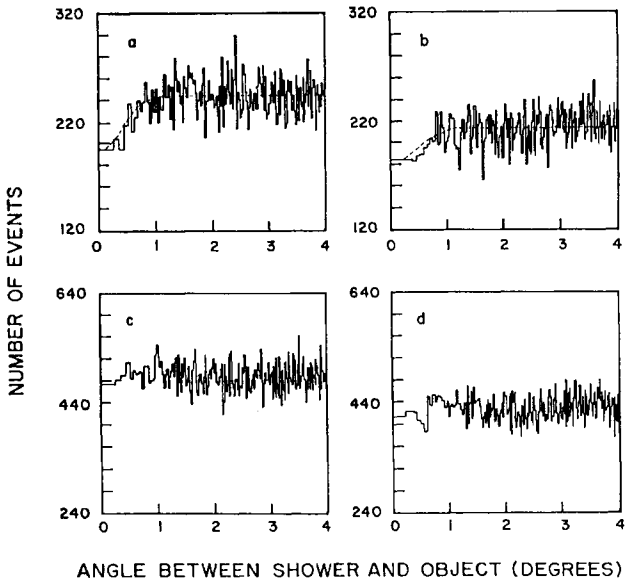

FIG. 3. The number of events in annuli of constant solid angle (the bin at the far left is $\frac{1}{4}°$ wide) centered on the (a) Moon, (b) Sun, (c) two fake Moons, and (d) two fake Suns, for those showers surviving a minimum shower size cut. The dashed line is the expected number of events with angular resolution determined from the likelihood analysis and normalized from fake sources.

TABLE II. Same data as in Table I, but with a minimum shower size cut of $\log_{10}$(shower size) > 4.5.

	Number of events in first bin	Number of background events	Significance of first bin deficit
Moon	195	244.0	3.1σ
Sun	184	213.8	2.0σ

better than that shown in Fig. 2. The background number of events near the fake objects is shown in Figs. 3(c) and 3(d). We give in Table II the number of background events, the number of events in the first bin of Figs. 3(a) and 3(b), and the significance of this first bin deficit.

Although the Moon and Sun have similar angular size, Tables I and II and Figs. 2 and 3 show a difference in their shadowing. To explore the issue of whether this is a solar magnetic field effect, we generate two-dimensional images of the Moon and Sun shadows in ecliptic coordinates as follows: For each shower satisfying the core cut, we compute ecliptic latitude differences (the ecliptic latitude of shower minus latitude of real and fake objects) and ecliptic longitude differences (the ecliptic longitude of shower minus longitude of real and fake objects). In $0.1°\times0.1°$ bins, we accumulate separately for the Moon and Sun two-dimensional histograms of ecliptic latitude difference versus longitude difference, minus the mean from the corresponding fake objects. Each bin is averaged with the $\pm0.4°\times\pm0.4°$ surrounding bins, suppressing noise at spatial frequencies beyond our instrument resolution. The net deficit in two dimensions is shown as contour density plots in Fig. 4 for the Moon (left) and Sun (right). Contour lines are at -30 showers/degree^2 intervals starting at -60 showers/degree.^{2} The Moon shadow is symmetric and centered at the position of the Moon; the Sun shadow is more irregular.

IV. ANGULAR RESOLUTION

The deficits shown in Fig. 3 are used to determine the angular resolution and a binning-independent estimate of the significance of the shadowing contribution from these objects. We use a likelihood method similar to that of Ref. [8], where, in anticipation of the good resolution apparent in Fig. 3, we replace the point object approximation for the Moon and Sun angular size by the extended object counterpart. We define the angular resolution σ_{63} as the cone half angle containing 63% of signal showers. Owing to different conventions, the angular resolutions reported in this study, given the assumptions in our likelihood function, should be divided by $\sqrt{2}$ for comparison with the resolutions reported in Ref. [8]. Similarly, since the resolutions reported in Ref. [9] are defined by the cone half angle containing 50% of signal showers, the resolutions reported in this study should be divided by 1.2 for comparison.

In constructing the likelihood function, we assume that for a given trial σ_{63}, the number of events in an annulus centered on the Moon or Sun is the sum of contributions from a flat background in $\cos\theta$ less a shadowing term, and is given by

$$\frac{dN}{d\cos\theta} = 1 - \int_{r=0}^{\theta_0}\int_{\phi=0}^{2\pi}\left[r\,dr\,d\phi\,\frac{1}{2\pi}\,\frac{2\pi}{2\pi\sigma^2}\exp\left[-\frac{\theta'^2}{2\sigma^2}\right]\right],$$

where the integration is over the solid angle subtended by the shadowing object. In this expression, $\sigma=\sigma_{63}/\sqrt{2}$, θ' is the space angle between the solid angle element $r\,dr\,d\phi$ and the shower direction, θ is the space angle between the center of the object and shower direction, and θ_0 is the angular radius of the Moon or Sun, as appropriate, at the time of the shower. This distribution of events assumes that the angular resolution is described by a symmetric two-dimensional Gaussian distribution. Up to a multiplicative constant, the probability to observe a shower at angle θ (out to maximum opening angle 4°) is then

$$\frac{dP}{d\cos\theta} = \frac{dN}{d\cos\theta}\,\frac{\int_{\cos0°}^{\cos4°} d\cos\theta}{\int_{\cos0°}^{\cos4°}(dN/d\cos\theta)\,d\cos\theta},$$

where the denominator normalizes the probability for each trial σ_{63} according to the number of events in the range 0° to 4°, and the numerator is a constant multiplicative factor shifting the large θ base line of the log likelihood to zero. The results presented here are insensitive

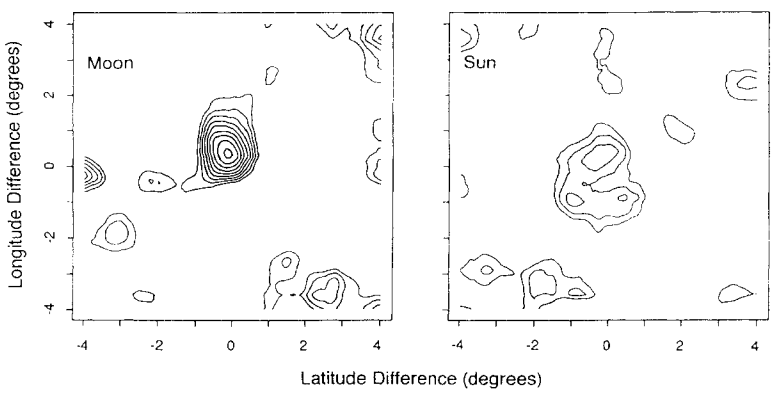

FIG. 4. The moon (left) and sun (right) deficit in two-dimensional ecliptic coordinates. The horizontal axis is the ecliptic latitude difference between the shower and object, the vertical axis is the longitudinal difference. Contour lines are at -30 showers/degree^2 intervals starting at -60 showers/degree^2.

to the exact value of the cone size up to about cos6°, where the constant background assumption begins to fail due to the steeply rising event yield with rising altitude.

The log likelihood as a function of trial resolution formed from the probabilities for each shower arriving within 4° space angle of the Moon and Sun are shown in Figs. 5(a) and 5(b). The most likely trial σ_{63} and the corresponding significance of the shadowing contribution in the likelihood is given in Table III (upper). The Moon has a 4.7σ likelihood maximum at $0.77^{+0.14}_{-0.10}$° (consistent with a Čerenkov telescope study of angular resolution [2]), and the Sun has a 4.8σ likelihood maximum at $0.89^{+0.20}_{-0.15}$°. The background likelihoods from fake objects, shown in Figs. 5(c) and 5(d), are consistent with no shadowing whatsoever.

For those 1.5 million events failing the 15 m core cut, a similar likelihood analysis yields the most probable trial σ_{63} and the significance of the shadowing term given in Table III (lower). The Moon has a 2.5σ likelihood maximum at $1.29^{+0.43}_{-0.27}$° and the Sun has a 2.3σ likehood maximum at $1.25^{+0.58}_{-0.34}$°.

We again consider those events surviving the 15 m core cut, where, in addition, events are grouped into shower size ranges $\log_{10}(\text{shower size}) < 4.2$, $4.2 < \log_{10}(\text{shower size}) < 4.5$, and $4.5 < \log_{10}(\text{shower size})$. The likelihood analysis, applied separately to events in each of these three groups, yields the most probable trial resolution and significance of the shadowing term as given in Table IV. We also compute a χ^2 between data binned in Fig. 3 (64 bins) and the predicted number of events from the angular resolution of Table IV, with normalization from the corresponding fake objects. This goodness of fit measure is sensitive to deviations from the flat background assumption in the likelihood. For events near the Sun, the

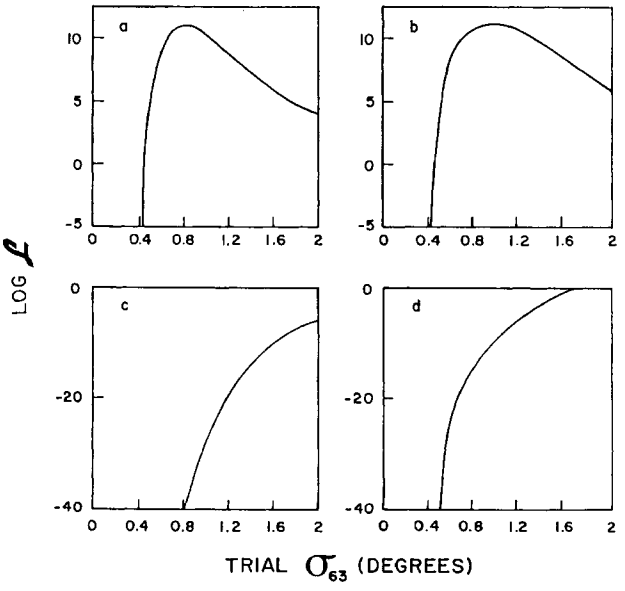

FIG. 5. The log likelihood versus trial angular resolution for the (a) Moon, (b) Sun, and backgrounds from (c) two fake Moons, and (d) two fake Suns for those showers surviving a 15 m core cut.

TABLE III. The angular resolution and significance of the shadowing term for events surviving and failing a 15 m core cut.

	σ_{63} (degrees)	Significance
Events surviving core cut		
Moon	$0.77^{+0.14}_{-0.10}$	4.7σ
Sun	$0.89^{+0.20}_{-0.15}$	4.8σ
Events failing core cut		
Moon	$1.29^{+0.43}_{-0.27}$	2.5σ
Sun	$1.25^{+0.58}_{-0.34}$	2.3σ

χ^2 is poor in the lower shower size range, and of marginal confidence in the intermediate shower size range. In the Moon sample, the χ^2 is of marginal confidence in the lower shower size range. This is not unexpected, for recall from the Introduction that solar and terrestrial magnetic fields cannot be entirely neglected (especially for cosmic rays with energy near the CASA threshold), and the CASA angular resolution is poor in the lower shower size range. At larger shower sizes (and thus at higher cosmic ray magnetic rigidity), the agreement between the form of the likelihood and the data is excellent. For example, the dashed line in Fig. 3 is the number of events predicted from combining angular resolutions of Table IV with normalization from fake Moons and Suns. The analysis was repeated with a two-dimensional Gaussian resolution function in horizon coordinates, and did not result in any appreciable change in the resulting angular resolution.

These likelihood studies use the exact expression for shadowing from an extended object. That the point object approximation is not sufficiently accurate is illustrated in the following: We repeat the likelihood analysis on events in the largest shower size range, with the shadowing term in the likelihood replaced by the point approximation. This increased the most likely angular resolution

TABLE IV. The angular resolution and significance of the shadowing term in three ranges of shower size. The χ^2 between data binned in Fig. 3 and the predicted number of events from the angular resolution of this table with normalization from the corresponding background data. There is a 15 m core cut applied to these data.

	σ_{63} (degrees)	Significance	χ^2
$\log_{10}(\text{shower size}) < 4.2$			
Moon	$1.78^{+0.73}_{-0.55}$	1.1σ	87.7
Sun	$1.96^{+0.84}_{-0.64}$	0.6σ	122.6
$4.2 < \log_{10}(\text{shower size}) < 4.5$			
Moon	$1.29^{+0.38}_{-0.26}$	2.8σ	63.6
Sun	$1.59^{+0.84}_{-0.43}$	1.8σ	90.5
$4.5 < \log_{10}(\text{shower size})$			
Moon	$0.49^{+0.07}_{-0.06}$	5.7σ	60.0
Sun	$0.58^{+0.11}_{-0.08}$	4.7σ	75.9

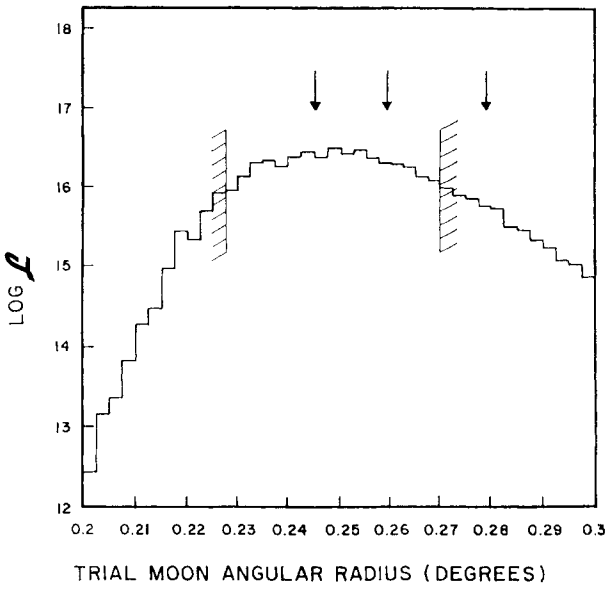

FIG. 6. The log likelihood versus trial angular radius of the Moon for those showers surviving a 15 m core cut and $4.5 < \log_{10}$(shower size). The 67% confidence interval of angular radii is indicated. The three arrows mark the average Moon angular radius, and angular radius at its apogee and perigee.

by almost 25%, demonstrating the importance of the finite sizes of the Moon and Sun in the likelihood. For events near the Moon in the largest shower size range, we fix in the likelihood the angular resolution at the value from Table IV, and treat the angular radius of the Moon as the trial variable. The log likelihood versus trial Moon angular radius is shown in Fig. 6. The 67% confidence interval of angular radii is indicated. The three arrows mark the average Moon angular radius, and angular radius at its apogee and perigee. The angular radius of the Moon measured thus by CASA is $0.25\pm0.02°$, consistent with its known average angular radius of 0.26° over the period of time when these data were taken.

V. CONCLUSIONS

We have seen the shadows of the Moon and Sun using cosmic rays with energies upwards of 100 TeV. The significance of the Moon shadowing for events with shower cores landing inside CASA is 4.7σ and the significance of the Sun shadowing is 4.8σ. This observation is not an artifact, as demonstrated by the lack of shadowing by fake Moons and Suns. The σ_{63} angular resolution for events near the Moon is $0.77^{+0.14}_{-0.10}°$, the σ_{63} angular resolution for events near the Sun is $0.89^{+0.20}_{-0.15}°$. The angular resolution is significantly worse for events falling outside the array boundary, and significantly better for larger showers. For $\log_{10}$(shower size) > 4.5, the σ_{63} angular resolution for events near the Moon is $0.49^{+0.07}_{-0.06}°$, and the σ_{63} angular resolution for events near the Sun is $0.58^{+0.11}_{-0.08}°$. The measured angular radius of the Moon is $0.25\pm0.02°$, in good agreement with its known value, demonstrating the importance of the finite size of the Moon and Sun in the likelihood.

The shadowing for the Sun is somewhat less significant than that of the Moon, and the flat background assumptions fails for small showers coming from Sun's direction. Further, the ecliptic two-dimensional moon shadow is symmetric and centered at the position of the moon; the sun shadow is irregular. This is likely due to rigidity dependent curvature of cosmic rays by the solar magnetic field, and indeed such effects are invoked to explain phenomena seen at lower energies [9]. However, quantitative interpretation of the Sun's shadow in terms of solar magnetic effects is difficult, as data for this analysis (and analyses of Refs. [8,9]) were taken when the solar magnetic field had small dipole moment with large contributions from higher multipoles [10]. It may be possible to fold in the array resolution and exposure with measured solar magnetic fields in order to determine whether the Sun's shadow is indeed influenced by the solar magnetic field.

ACKNOWLEDGMENTS

We gratefully acknowledge the help and support of the staff of the Dugway Proving Ground, as well as helpful discussions with Eugene N. Parker. This work was supported by the National Science Foundation, the Department of Energy, The Grainger Foundation, and the Alfred P. Sloan Foundation.

[1] A. Borione *et al.*, Nucl. Instrum. Methods (to be published).

[2] L. J Rosenberg, in *High Energy Gamma-Ray Astronomy (Ann Arbor, MI, 1990)*, Proceedings of the International Conference, edited by James Matthews, AIP, Conf. Proc. No. 220 (AIP, New York, 1990), p. 111.

[3] Rene A. Ong, in *Physics and Experimental Techniques of High Energy Neutrinos and VHE and UHE Gamma-Ray Particle Physics*, Proceedings of the Workshop, Little Rock, Arkansas, 1989, edited by G. B. Yodh, D. V. Wold, and W. Kropp [Nucl. Phys. B (Proc. Suppl.) **14A**, 273 (1990)].

[4] K. G. Gibbs, Nucl. Instrum. Methods A **264**, 67 (1988).

[5] J. W. Cronin *et al.*, Phys. Rev. D **45**, 4385 (1992).

[6] A review of the observational status of putative sources is D. J. Fegan, in *Proceedings of the 21st International Cosmic Ray Conference*, Adelaide, Australia, 1989, edited by R. J. Protheroe (Graphic Services, Northfield, South Aus-

tralia, 1990), Vol. 11, p. 23.
[7] G. W. Clark, Phys. Rev. **108**, 450 (1957).
[8] D. E. Alexandreas *et al.*, Phys. Rev. D **43**, 1735 (1991).
[9] N. Amenomori *et al.*, Phys. Rev. D **47**, 2657 (1993).
[10] J. T. Hoeksema, John M. Wilcox Solar Observatory at Stanford Report No. CSSA-ASTRO-91-01 (unpublished), Vol. 2.
[11] *The Astronomical Almanac* (U.S. Government Printing Office, Washington, D.C., and Her Majesty's Stationery Office, London, 1990, 1991, 1992).
[12] T. Li and Y. Ma, Astrophys. J. **272**, 317 (1983).